

Article

Direct Observation of Carrier Transportation between Localized States in InGaN Quantum Wells

Yangfeng Li ¹, Yixiao Li ^{1,2}, Jie Zhang ^{3,*}, Yi Wang ^{1,2}, Tong Li ^{1,2}, Yang Jiang ^{4,*}, Haiqiang Jia ^{4,5}, Wenxin Wang ^{4,5}, Rong Yang ^{1,2,*} and Hong Chen ^{4,5}

¹ College of Semiconductors (College of Integrated Circuits), Hunan University, Changsha 410082, China

² School of Physics and Electronics, Hunan University, Changsha 410082, China

³ Hunan San'an Semiconductor Co., Ltd., Changsha 410000, China

⁴ Key Laboratory for Renewable Energy, Beijing Key Laboratory for New Energy Materials and Devices, Beijing National Laboratory for Condensed Matter Physics, Institute of Physics, Chinese Academy of Sciences, Beijing 100190, China

⁵ Songshan Lake Materials Laboratory, Dongguan 523808, China

* Correspondence: authors: jack_zhang@sanan-ic.com (J.Z.); jiangyang@iphy.ac.cn (Y.J.); yangrong@hnu.edu.cn (R.Y.)

Abstract: Despite the large misfit dislocation densities, indium gallium nitride (InGaN) demonstrates high luminous efficiency both for electroluminescence and photoluminescence. The mechanism behind it has been interpreted as the existence of potential minima (i.e., localized states), which will screen the non-radiative recombination centers to avoid carriers being trapped by the defects. The existence of localized states has been testified by many experiments. However, almost all of the observations are indirect observations, and some experiments, such as those focused on whether the indium clusters observed by transmission electron microscopy are localized states, still remain controversial. Here, we report the direct observation of carrier transportation between localized states driven by temperature-dependent photoluminescence (TDPL) and excitation power-dependent PL in InGaN quantum wells. This enriches the experimental evidence on the existence of localized states.

Keywords: InGaN; localized states; TDPL; excitation power-dependent PL



Citation: Li, Y.; Li, Y.; Zhang, J.; Wang, Y.; Li, T.; Jiang, Y.; Jia, H.; Wang, W.; Yang, R.; Chen, H. Direct Observation of Carrier

Transportation between Localized States in InGaN Quantum Wells.

Crystals **2022**, *12*, 1837. <https://doi.org/10.3390/cryst12121837>

Academic Editors: Igor Yurkevich, Zeyu Liu, Mingzeng Peng, Yang Wang and Yuanpeng Wu

Received: 28 November 2022

Accepted: 14 December 2022

Published: 16 December 2022

Publisher's Note: MDPI stays neutral with regard to jurisdictional claims in published maps and institutional affiliations.



Copyright: © 2022 by the authors. Licensee MDPI, Basel, Switzerland. This article is an open access article distributed under the terms and conditions of the Creative Commons Attribution (CC BY) license (<https://creativecommons.org/licenses/by/4.0/>).

1. Introduction

The transcendental optoelectronic properties of indium gallium nitride (InGaN) enable the prevailing application and development of InGaN-based devices in solid-state lighting [1–6], micro light-emitting diode (μ LED) displays [7,8], light communication [9,10], etc. Since the early research stages for InGaN, the high luminous efficiency accompanied by high misfit defects (e.g., the threading dislocation density in the magnitude order of $\sim 10^8$ – 10^9 cm⁻²) has attracted much attention from researchers, seeking to interpret such a contradictory phenomenon. Chichibu et al. suggest the existence of potential minima in the InGaN materials, which will localize the carriers spatially, thus avoiding carrier consumption via non-radiative recombination centers caused by defects [11]. The main experimental evidence includes a large Stokes shift between the photoluminescence (PL) peak and the absorption peak given by the photoluminescence excitation (PLE), and also the energy deviation between the electroluminescence (EL) peak and the modulated electroabsorption (EA) spectra [12]. In addition, the blue shift of the EL peak under a high injection current also indicates the band filling of the localized states. A long decay time (\sim ns) obtained from the time-resolved PL (TRPL) measurements also implies the carrier's transportation towards localized states. Moreover, the decay time elongates at the lower-energy side of the emission peak, in agreement with the localized state-induced band-tail distribution of carriers [13]. According to the cathodoluminescence (CL) results, a small-area scan demonstrates sharp peaks with narrower full-width at half-maximum (FWHM) values, which also

reveals spatial potential fluctuations [12]. However, due to the limited spatial resolution of CL measurement, the size of localized states could only be estimated to be smaller than 60 nm [14]. Eliseev et al. proposed a model to quantitatively evaluate the degree of localized states and suggested that an S-shaped curve, which is demonstrated by the evolution of the PL peak with increasing temperature, should be considered evidence of the carrier's transportation between deep and shallow localized states [15]. As the possible mechanisms causing localized states include thickness undulation and composition fluctuation (most probably caused by phase separation) [16], transmission electron microscopy (TEM) is widely used to provide direct evidence of the localized states [11]. A number of researchers have observed indium clusters with a lateral size in several to tens of nanometers in the InGaN quantum well (QW), and such a morphology, with a higher indium composition than that of the adjoining sections, is usually interpreted as a localized state [2,11,17]. However, other researchers suggest that the indium clusters should not be localized states. Lefebvre et al. found that the S-shaped curve even exists in the InGaN quantum box; then, they concluded that the spatial extension of localized states should be smaller than the size of the quantum box (5–10 nm) [18]. Graham et al. suggested that the in-plane length of localized states should be ~2 nm according to the analyses of the longitudinal-optical (LO) phonon replicas [19]. Moreover, they attributed the formation of localized states to the well-width fluctuations. Smeeton et al. pointed out that the indium clusters were most probably false images, as they will emerge with a prolonged electron irradiation time or when exposed to a high-voltage electron beam [20]. The possible mechanisms may be attributable to radiolysis and knock-on damage, which cause the lattice distortion of InGaN, resulting in an electron-beam-induced strain [21]. Other researchers used the three-dimensional atom probe (3DAP) technique to analyze the atom distribution of InGaN multiple-quantum wells (MQWs) and found that the indium distribution coincides with the binomial distribution that occurs in random ternary alloys [22,23]. They stated that an inhomogeneous indium distribution was not observed and suggested that the localized states should be a result of well-width fluctuations [22]. Galtrey et al. further explained that localized states are a result of QW width fluctuations, which are caused by a surface-segregated indium layer [24,25]. As a result, the observation of localized states from TEM becomes a less convincing method. Thereafter, the localized states were further attributed to the atomic condensates of In–N via analyses of implanted positron annihilation experimental results [26].

In 2019, we reported the experimental results of carrier transportation between different localized states as the temperature was ramped up from 10 K to 300 K in a single yellow-green QW [27]. Such a study offers more concrete evidence for the existence of localized states. However, as the energy difference between the two localized states was ~70 meV, it was difficult to distinguish the integrated intensity for each peak exactly. In this study, we fabricated three InGaN MQWs, which were subjected to an in-situ post-annealing process after the growth of each QW to establish quantum-dot-like states. From the temperature-dependent PL (TDPL) and excitation power-dependent PL measurements, we directly observed the carrier's transport from the deep localized states to the relatively shallow localized states as the temperature or the excitation power increased. The results provide a vivid picture of the existence of localized states.

2. Materials and Methods

Three MQWs were grown on a 350-nm-thick GaN template following an aluminum nitride (AlN) buffer layer composed of a 15-nm low-temperature AlN and a 300-nm high-temperature AlN on a 2-inch silicon (111) substrate by metal organic chemical vapor deposition (MOCVD). The detailed growth conditions for the GaN template on the silicon substrate can be found in our previous study [28]. To assess the presence of quantum dots (QDs) in the QW, we exploited the in-situ post-annealing method, which is also called the growth interruption method, to evaporate the indium clusters surrounding defects and facilitate the formation of quantum-dot-like localized states after the ending of each

QW [29–31]. The three QWs underwent the same growth conditions. Lastly, a 50-nm GaN was deposited as the capping layer. The schematic structure is shown in Figure 1. The TDPL were taken by a 325-nm He-Cd continuous-wavelength laser with the sample mounted on the cold finger of a closed-cycle helium compressor. The temperature could be changed from ~15 K to 300 K consecutively. The excitation power-dependent PL was carried out with the same setup, with the excitation power adjusted by a neutral optical attenuator at different temperatures (viz. 15 K, 70 K, 150 K, and 300 K) [32]. The TEM images were obtained via a JEM 2100Plus microscope, where the lamella was mechanically thinned, followed by further thinning by argon ions with a Gatan precision ion polishing system (PIPS). The voltage of TEM was kept at 200 kV.

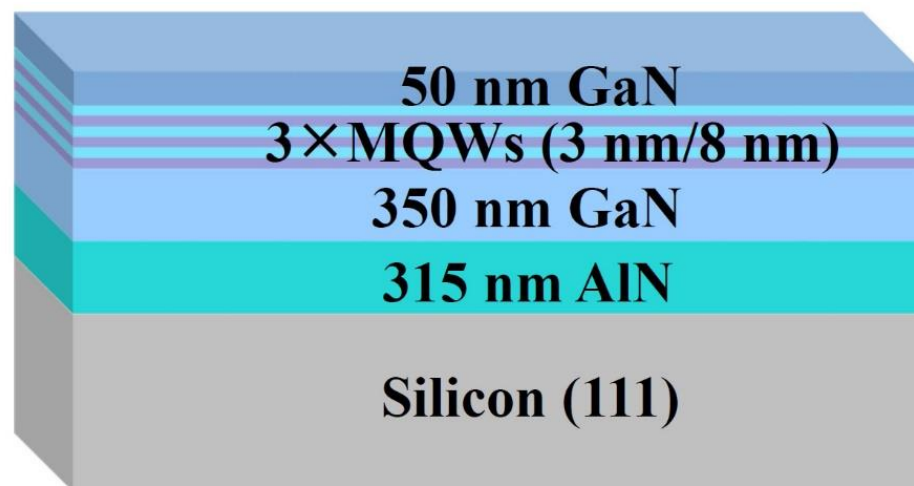


Figure 1. The schematic illustration of the InGaN MQW structure.

3. Results and Discussion

An example of the PL spectra obtained from 15 K to 300 K is presented in Figure 2a. At lower temperatures (15 K–~60 K), four emission peaks are obviously distinguishable, which are attributable to the emissions from deep localized states (P_L), shallow localized states (P_H), the wetting layer (P_W), and GaN (P_{GaN}), respectively. With increasing temperature, the P_{GaN} quenches rapidly and becomes indistinguishable at 300 K. The P_W also decays rapidly and disappears at the relatively lower excitation power at 300 K. A noticeable emission intensity change from P_L to P_H can be easily observed, as shown in Figure 2a. For a more detailed study, the spectra at each temperature are fitted by a multiple-peak curve fit with a Gaussian function. The exemplary fitted curves, as well as the experimentally obtained spectra at 15 K and 300 K, are depicted in Figure 2b, where the black lines are the measured data, the green lines are the fitted lines for each emission peak, and the red lines are the sums of all the green lines. The extracted relative PL-integrated intensities of the three emission peaks are delineated in Figure 2c. The relative PL-integrated intensity for a certain peak at each temperature is obtained by calculating the proportion of the absolute PL-integrated intensity of this peak in the sum of the absolute PL-integrated intensity for the three peaks. According to Figure 2c, the relative PL-integrated intensity of P_H remains on an increasing trajectory along with the increase in temperature, while those of P_L and P_W are liable to a monotonous decrease as the temperature ramps up. According to the changing tendency of the relative PL-integrated intensity, we infer that as the temperature increases, the carriers will gain enough kinetic energy to overcome the restriction of the deep localized states, thus causing a weakened PL emission of P_L . The consecutive increase in P_H emission among the three peaks implies that the thermally activated carriers tend to accumulate in the shallow localized state (i.e., P_H). It is worth noting that the absolute PL-integrated intensity of all the peaks decreases with the temperature increase. This could be due to the thermally activated non-radiative recombination centers, which consume the carriers, thus weakening the emission efficiency [4,30]. However, as the growth conditions are the same

for the three QWs, the deep and shallow localized states should be randomly distributed in the MQWs; then, the effects of the non-radiative recombination centers on both peaks should be equal at each temperature. In this case, the increase in the relative PL-integrated intensity in P_H is mainly due to the carrier's transportation from deep localized state (P_L). As the relative emission intensity of the wetting layer also demonstrates a decrease with temperature, the carrier transportation from P_W to P_H also cannot be excluded.

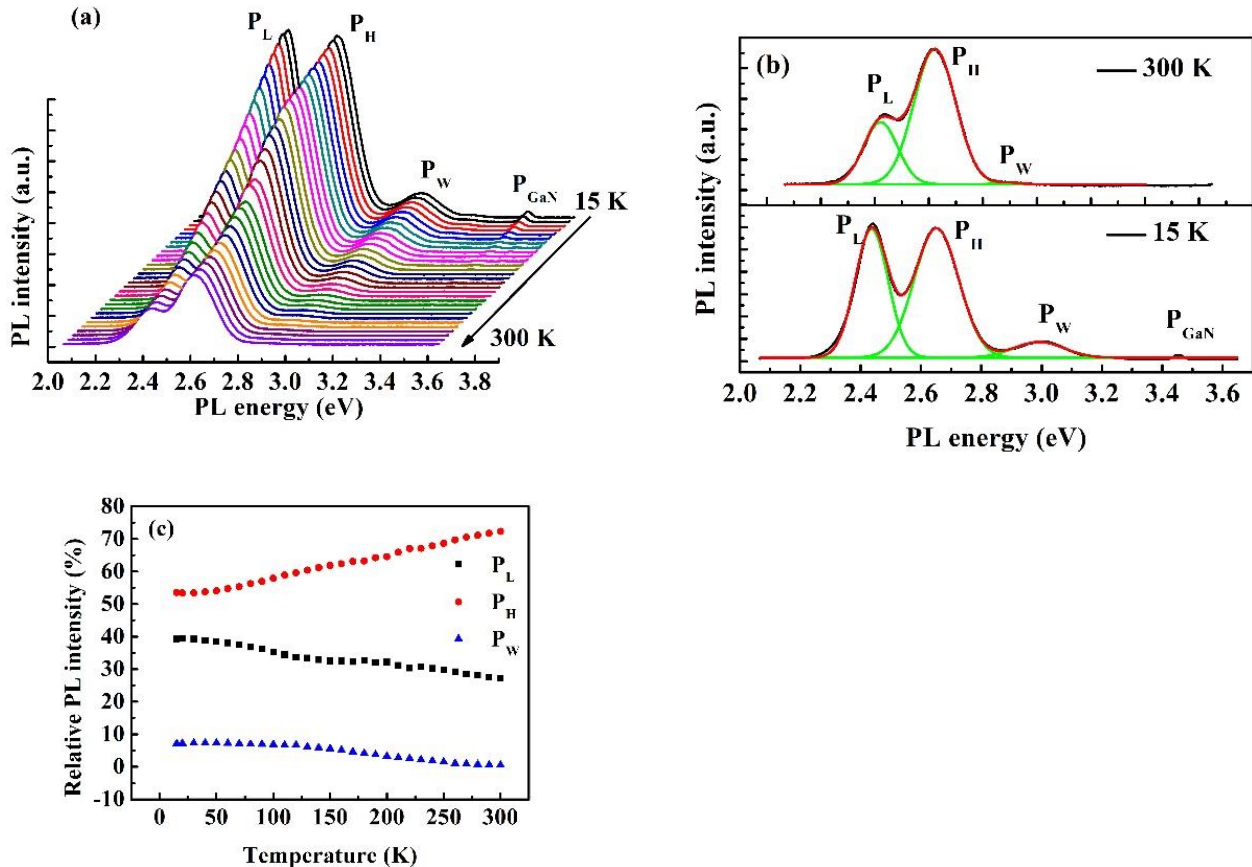


Figure 2. (a) The TDPL spectra from 15 K to 300 K. P_L , P_H , P_W , and P_{GaN} denote the emission peaks of the deep localized states (lower energy), shallow localized states (higher energy), wetting layer, and GaN, respectively. (b) The spectra as well as the fitting curves at 15 K and 300 K. The green lines are the fitted lines for each peak, while the red lines are the gross fitted lines for the whole spectrum. (c) The relative PL intensity for P_L , P_H , and P_W at different temperatures.

For a further study of the carrier transportation behavior, and to evaluate the non-radiative recombination centers in each peak at different temperatures, the excitation power-dependent PL was carried out at 15 K, 70 K, 150 K, and 300 K, respectively, with the excitation power being increased from 0.2 mW to 8 mW. Figure 3a,d,g,j present the spectral evolution under different excitation powers at 15 K, 70 K, 150 K, and 300 K, respectively. All the four peaks could clearly be distinguished due to the high radiative recombination efficiency at lower temperature, viz. 15 K. The peaks of P_L , P_H , and P_W are fitted by a Gaussian function, similarly to the treatment of the TDPL spectra; thus, the integrated intensities are extracted. As the P_W is submerged into the background noise in 300 K, only P_L and P_H could be well fitted through the excitation power range; thus, the data of P_W are absent at 300 K. The PL-integrated intensity obeys a power-law evolution with the excitation power, viz. $I \propto P^m$, where I represents the PL-integrated intensity, P denotes the excitation power, and m is the index. If radiative recombination dominates the recombination process, the index m is expected to be close to 1. If non-radiative recombination plays an important role in the recombination process, then the index m will be larger than 1, as the non-radiative recombination centers will not be effectively saturated

by the excited carriers under relatively low excitation powers [33,34]. The experimental data in Figure 3b,e,h,k are offset for clarity; therefore, they are not equal to the absolute PL-integrated intensities for P_L , P_H , and P_W . The fitted index m values for the three peaks (only two peaks at 300 K) are all close to 1 from 15 K to 300 K, and the values of m for each peak remain a small deviation at different temperatures. Such a phenomenon indicates that the recombination mechanism is analogous at different temperatures for each peak, confirming the assumption that the effects of the non-radiative recombination centers on all peaks are equivalent at each temperature. In addition, as the values of m are all close to 1, radiative recombination should dominate the recombination process in all three peaks. Therefore, the evolution of the PL-integrated intensity with temperature is mainly caused by the carrier transportation rather than the different non-radiative recombination processes in each peak. A more obvious carrier transportation between different localized states could be found in the evolution of the relative PL-integrated intensities with excitation power. The relative PL-integrated intensities of P_H and P_W maintain an increasing trend, whereas that of P_L diminishes monotonously, as shown in Figure 3c,f,i,j. Moreover, from Figure 3c,f, we find that, at lower excitation powers (0.2–1 mW), the relative PL-integrated intensity of P_L is the highest. This indicates that, at lower excitation powers, due to the deficiency of activated carriers, the photo-activated carriers are likely to fill the deep localized states as a first priority, thus generating the strongest emission from the deep localized states. When the excitation power increases to a certain level, the spillover carriers will fill the shallow localized states and the wetting layer, resulting in an enhancement in the emission intensities of P_H and P_W . As the peaks are somewhat weak under 0.2 mW excitation at 150 K, the PL-integrated intensity at 0.2 mW for P_L and P_W may suffer from an inaccurate evaluation because the peaks are difficult to be extracted from the background noise. Therefore, the data at 0.2 mW in Figure 3i show a deviation from the tendency in Figure 3c,f. However, as the PL signals are strong enough at higher excitation powers, the other data in Figure 3i are in agreement with those at other temperatures. As the P_W peak is severely weakened at 300 K, especially under lower excitation powers, only P_L and P_H are investigated at this temperature. From Figure 3k, it is verified that both P_L and P_H are dominated by the radiative recombination process. The monotonous decrease in the relative PL-integrated intensity of P_L and the concomitant increase in P_H in Figure 3l are indicators of the carrier transportation between different localized states. As the temperature of 300 K is relatively high, the carrier transportation behavior becomes more prominent.

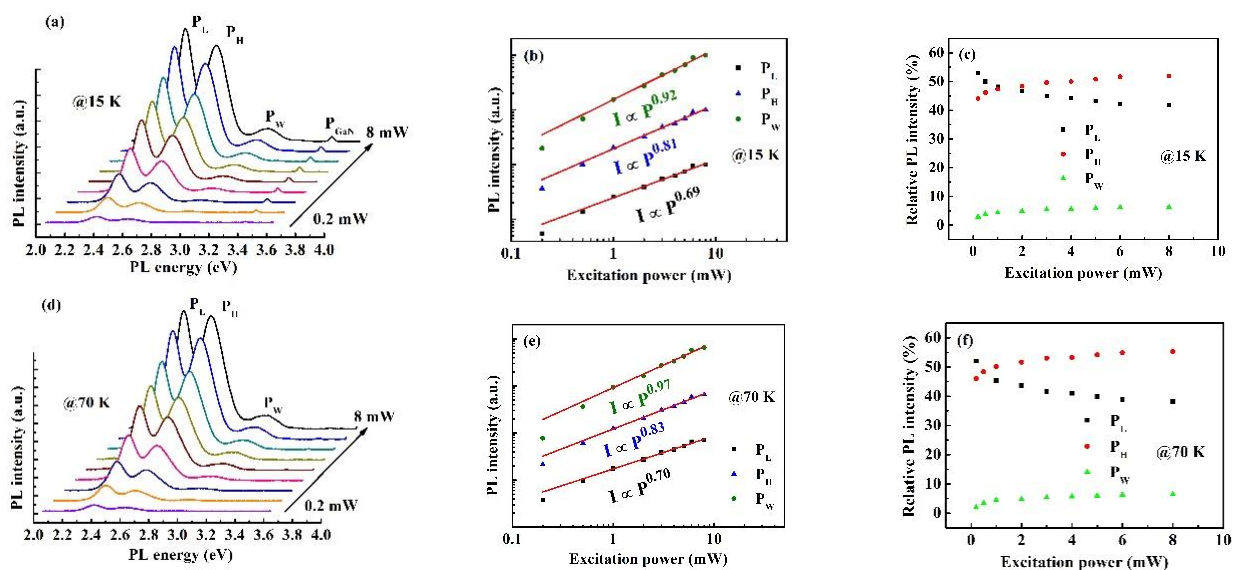


Figure 3. Cont.

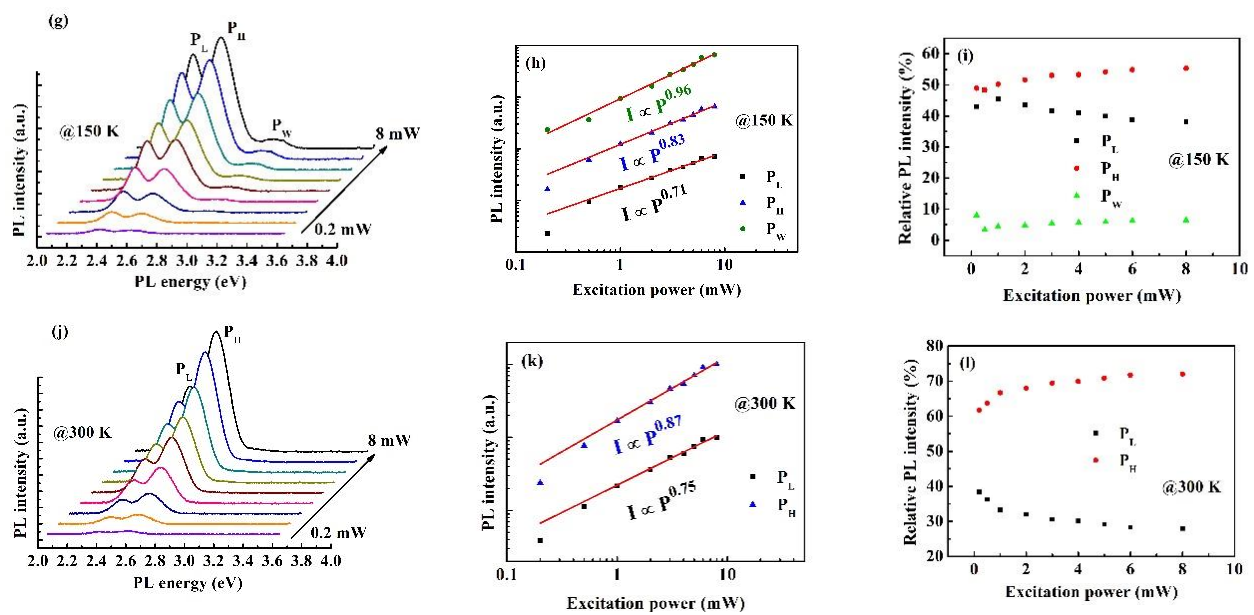


Figure 3. (a,d,g,j) The excitation power-dependent PL spectra at 15 K, 70 K, 150 K, and 300 K, respectively. (b,e,h,k) The PL-integrated intensity versus the excitation power at 15 K, 70 K, 150 K, and 300 K, respectively. The red lines are the fitted lines obeying a power law. The PL-integrated intensities are offset for clarity. (c,f,i,l) The relative PL-integrated intensity of the emission peaks under different excitation powers at 15 K, 70 K, 150 K, and 300 K, respectively.

The TEM images of the as-grown sample are presented in Figure 4. Figure 4a illustrates the stacking structure of the sample. Three MQWs with non-consecutive regions are sandwiched between the GaN template and the capping layer. In Figure 4b, one can clearly observe the morphology of the unambiguous quantum-dot-like blotches in the QWs. As the acceleration voltage was not high (200 kV), an aperture slot was added before the objective lens, and the electron spot was dispersed to a rather weak extent, we tend to accept such features to be the real characteristics of the material. In addition, we captured the images less than 10 s after exposure, and we also could not observe a morphology change as the exposure time elapsed. A further magnified image of the MQW region is shown in Figure 4c, where the quantum-dot-like speckles were measured to be 2.5–4.2 nm in width and 2.8–5 nm in height. Such quantum-dot-like structures may contribute to the formation of localized states.

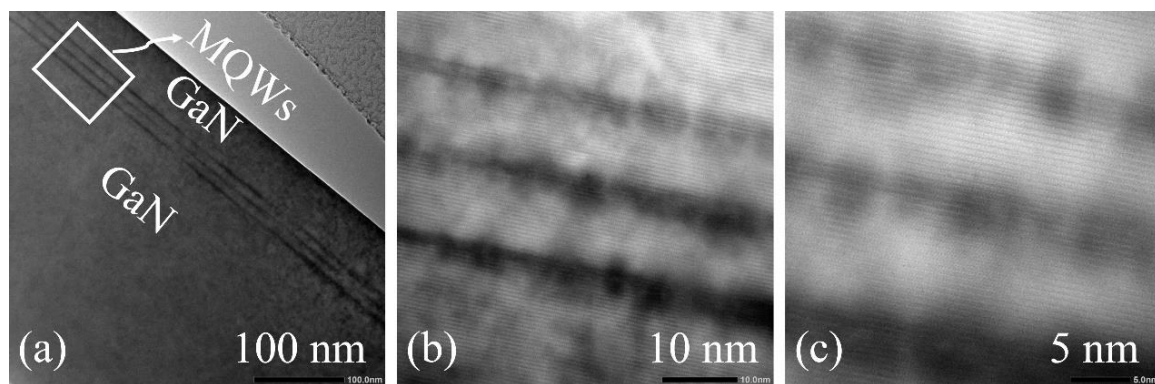


Figure 4. (a) The TEM image of the as-grown sample. Three MQWs with non-consecutive regions are noticeable. (b) The zoomed-in picture in the MQW region. Quantum-dot-like blotches are distinguishable. (c) A further magnified image of the MQW region. The quantum-dot-like speckles were measured to be 2.5–4.2 nm in width and 2.8–5 nm in height.

4. Conclusions

In conclusion, the carrier transportation between deep and shallow localized states is directly observed by TDPL and excitation power-dependent PL. The transportation behavior is further verified by the excitation power-dependent PL at different temperatures, where all the emission peaks are confirmed to be dominated by the radiative recombination process. The TEM images demonstrate a large number of quantum-dot-like blotches, which may contribute to the formation of localized states. This study enriches the evidence from experiments supporting the localized state assumption in InGaN QWs.

Author Contributions: Y.L. (Yangfeng Li) proposed and conducted the overall project. Y.L. (Yixiao Li), Y.W. and T.L. contributed to the methodology. Y.L. (Yixiao Li), Y.W. and T.L. contributed to the validation. J.Z., Y.J., H.J., W.W., R.Y. and H.C. supervised. J.Z., Y.J., H.J., W.W., R.Y. and H.C. obtained the funding support. Y.L. (Yangfeng Li) provided the crystal growth; performed the TDPL and excitation-power dependent PL measurements, TEM sample preparation, TEM measurements, and data analysis; and composed the manuscript. All authors have read and agreed to the published version of the manuscript.

Funding: This work was supported by the National Science Foundation of China (NSFC) (grant numbers 62122084, 12074412, 62150027, and 61991441), the Strategic Priority Research Program of Chinese Academy of Sciences (grant number XDB33000000), the Fundamental Research Funds for the Central Universities (grant number 531118010804), and the Education Department of Hunan Province (grant number 22B0020).

Data Availability Statement: The data that support the findings of this study are available from the corresponding author upon reasonable request.

Acknowledgments: We thank Ziguang Ma from the Institute of Physics, Chinese Academy of Sciences, for the discussion of the experimental results. We are indebted to Professor Aizi Jin from the Institute of Physics, Chinese Academy of Sciences, for providing the facility for TEM sample fabrication, and Professor Ying Li, Huanfang Tian, and Xin'an Yang from the Institute of Physics, Chinese Academy of Sciences, for the TEM test.

Conflicts of Interest: The authors declare no conflict of interest.

References

1. Schubert, E.F.; Kim, J.K. Solid-State Light Sources Getting Smart. *Science* **2005**, *308*, 5726. [[CrossRef](#)] [[PubMed](#)]
2. Wang, L.; Wang, L.; Yu, J.; Hao, Z.; Luo, Y.; Sun, C.; Han, Y.; Xiong, B.; Wang, J.; Li, H. Abnormal Stranski-Krastanov Mode Growth of Green InGaN Quantum Dots: Morphology, Optical Properties, and Applications in Light-Emitting Devices. *ACS Appl. Mater. Interfaces* **2019**, *11*, 1228–1238. [[CrossRef](#)] [[PubMed](#)]
3. Iida, D.; Zhuang, Z.; Kirilenko, P.; Velazquez-Rizo, M.; Najmi, M.A.; Ohkawa, K. 633-nm InGaN-based red LEDs grown on thick underlying GaN layers with reduced in-plane residual stress. *Appl. Phys. Lett.* **2020**, *116*, 162101. [[CrossRef](#)]
4. Li, Y.; Liu, C.; Zhang, Y.; Jiang, Y.; Hu, X.; Song, Y.; Su, Z.; Jia, H.; Wang, W.; Chen, H. Realizing Single Chip White Light InGaN LED via Dual-Wavelength Multiple Quantum Wells. *Materials* **2022**, *15*, 3998. [[CrossRef](#)]
5. Li, Y.; Jiang, Y.; Jia, H.; Wang, W.; Yang, R.; Chen, H. Superior Optoelectronic Performance of N-Polar GaN LED to Ga-Polar Counterpart in the "Green Gap" Range. *IEEE Access* **2022**, *10*, 95565. [[CrossRef](#)]
6. Jiang, Y.; Li, Y.; Li, Y.; Deng, Z.; Lu, T.; Ma, Z.; Zuo, P.; Dai, L.; Wang, L.; Jia, H.; et al. Realization of high-luminous-efficiency InGaN light-emitting diodes in the green gap range. *Sci. Rep.* **2015**, *5*, 10883. [[CrossRef](#)]
7. Meng, W.; Xu, F.; Yu, Z.; Tao, T.; Shao, L.; Liu, L.; Li, T.; Wen, K.; Wang, J.; He, L.; et al. Three-dimensional monolithic micro-LED display driven by atomically thin transistor matrix. *Nat. Nanotechnol.* **2021**, *16*, 1231–1236. [[CrossRef](#)]
8. Hwangbo, S.; Hu, L.; Hoang, A.T.; Choi, J.Y.; Ahn, J.H. Wafer-scale monolithic integration of full-colour micro-LED display using MoS(2) transistor. *Nat. Nanotechnol.* **2022**, *17*, 500–506. [[CrossRef](#)]
9. Wang, L.; Wei, Z.; Chen, C.-J.; Wang, L.; Fu, H.Y.; Zhang, L.; Chen, K.-C.; Wu, M.-C.; Dong, Y.; Hao, Z.; et al. 1.3 GHz E-O bandwidth GaN-based micro-LED for multi-gigabit visible light communication. *Photonics Res.* **2021**, *9*, 792. [[CrossRef](#)]
10. Li, G.; Hu, F.; Zou, P.; Wang, C.; Lin, G.R.; Chi, N. Advanced Modulation Format of Probabilistic Shaping Bit Loading for 450-nm GaN Laser Diode based Visible Light Communication. *Sensors* **2020**, *20*, 6143. [[CrossRef](#)]
11. Chichibu, S.; Azuhata, T.; Sota, T.; Nakamura, S. Spontaneous emission of localized excitons in InGaN single and multiquantum well structures. *Appl. Phys. Lett.* **1996**, *69*, 4188. [[CrossRef](#)]
12. Chichibu, S.; Sota, T.; Wada, K.; Nakamura, S. Exciton localization in InGaN quantum well devices. *J. Vac. Sci. Technol. B* **1998**, *16*, 2204. [[CrossRef](#)]

13. Narukawa, Y.; Kawakami, Y.; Fujita, S.; Fujita, S.; Nakamura, S. Recombination dynamics of localized excitons in In_{0.20}Ga_{0.80}N-In_{0.05}Ga_{0.95} multiple quantum wells. *Phys. Rev. B* **1997**, *55*, R1938–R1941. [[CrossRef](#)]
14. Chichibu, S.; Wada, K.; Nakamura, S. Spatially resolved cathodoluminescence spectra of InGaN quantum wells. *Appl. Phys. Lett.* **1997**, *71*, 2346. [[CrossRef](#)]
15. Eliseev, P.G.; Perlin, P.; Lee, J.; Osifski, M. “Blue” temperature-induced shift and band-tail emission in InGaN-based light sources. *Appl. Phys. Lett.* **1997**, *71*, 569–571. [[CrossRef](#)]
16. Ho, I.-h.; Stringfellow, G.B. Solid phase immiscibility in GaInN. *Appl. Phys. Lett.* **1996**, *69*, 2701. [[CrossRef](#)]
17. Narukawa, Y.; Kawakami, Y.; Funato, M.; Fujita, S.; Fujita, S.; Nakamura, S. Role of self-formed InGaN quantum dots for exciton localization in the purple laser diode emitting at 420 nm. *Appl. Phys. Lett.* **1997**, *70*, 981–983. [[CrossRef](#)]
18. Lefebvre, P.; Taliercio, T.; Morel, A.; Allègre, J.; Gallart, M.; Gil, B.; Mathieu, H.; Damilano, B.; Grandjean, N.; Massies, J. Effects of GaAlN barriers and of dimensionality on optical recombination processes in InGaN quantum wells and quantum boxes. *Appl. Phys. Lett.* **2001**, *78*, 1538–1540. [[CrossRef](#)]
19. Graham, D.M.; Soltani-Vala, A.; Dawson, P.; Godfrey, M.J.; Smeeton, T.M.; Barnard, J.S.; Kappers, M.J.; Humphreys, C.J.; Thrush, E.J. Optical and microstructural studies of InGaN/GaN single-quantum-well structures. *J. Appl. Phys.* **2005**, *97*, 103508. [[CrossRef](#)]
20. Smeeton, T.M.; Kappers, M.J.; Barnard, J.S.; Vickers, M.E.; Humphreys, C.J. Electron-beam-induced strain within InGaN quantum wells: False indium “cluster” detection in the transmission electron microscope. *Appl. Phys. Lett.* **2003**, *83*, 5419. [[CrossRef](#)]
21. Smeeton, T.M.; Humphreys, C.J.; Barnard, J.S.; Kappers, M.J. The impact of electron beam damage on the detection of indium-rich localisation centres in InGaN quantum wells using transmission electron microscopy. *J. Mater. Sci.* **2006**, *41*, 2729–2737. [[CrossRef](#)]
22. Galtrey, M.J.; Oliver, R.A.; Kappers, M.J.; Humphreys, C.J.; Stokes, D.J.; Clifton, P.H.; Cerezo, A. Three-dimensional atom probe studies of an In_xGa_{1-x}N / GaN multiple quantum well structure: Assessment of possible indium clustering. *Appl. Phys. Lett.* **2007**, *90*, 061903. [[CrossRef](#)]
23. Bennett, S.E.; Saxey, D.W.; Kappers, M.J.; Barnard, J.S.; Humphreys, C.J.; Smith, G.D.; Oliver, R.A. Atom probe tomography assessment of the impact of electron beam exposure on In_xGa_{1-x}N / GaN quantum wells. *Appl. Phys. Lett.* **2011**, *99*, 021906. [[CrossRef](#)]
24. Galtrey, M.J.; Oliver, R.A.; Kappers, M.J.; Humphreys, C.J.; Clifton, P.H.; Larson, D.; Saxey, D.W.; Cerezo, A. Three-dimensional atom probe analysis of green- and blue-emitting In_xGa_{1-x}N / GaN multiple quantum well structures. *J. Appl. Phys.* **2008**, *104*, 013524. [[CrossRef](#)]
25. Northrup, J.E.; Walle, C.G.V.d. Indium versus hydrogen-terminated GaN(0001) surfaces: Surfactant effect of indium in a chemical vapor deposition environment. *Appl. Phys. Lett.* **2004**, *84*, 4322. [[CrossRef](#)]
26. Chichibu, S.F.; Uedono, A.; Onuma, T.; Haskell, B.A.; Chakraborty, A.; Koyama, T.; Fini, P.T.; Keller, S.; Denbaars, S.P.; Speck, J.S.; et al. Origin of defect-insensitive emission probability in In-containing (Al,In,Ga)N alloy semiconductors. *Nat. Mater.* **2006**, *5*, 810–816. [[CrossRef](#)]
27. Li, Y.; Deng, Z.; Ma, Z.; Wang, L.; Jia, H.; Wang, W.; Jiang, Y.; Chen, H. Visualizing carrier transitions between localization states in a InGaN yellow–green light-emitting-diode structure. *J. Appl. Phys.* **2019**, *126*, 095705. [[CrossRef](#)]
28. Li, Y.; Tang, C.W.; Lau, K.M. Comparison of the AlN and GaN crystalline quality on 2-inch silicon substrate via two growth methods. *J. Cryst. Growth* **2020**, *535*, 125545. [[CrossRef](#)]
29. Li, Y.; Jin, Z.; Han, Y.; Zhao, C.; Huang, J.; Tang, C.W.; Wang, J.; Lau, K.M. Surface morphology and optical properties of InGaN quantum dots with varying growth interruption time. *Mater. Res. Express* **2020**, *7*, 015903. [[CrossRef](#)]
30. Zhu, Y.; Lu, T.; Zhou, X.; Zhao, G.; Dong, H.; Jia, Z.; Liu, X.; Xu, B. Origin of huge photoluminescence efficiency improvement in InGaN GaN multiple quantum wells with low-temperature GaN cap layer grown in N₂/H₂ mixture gas. *Appl. Phys. Express* **2017**, *10*, 061004. [[CrossRef](#)]
31. Woolf, A.; Puchter, T.; Aharonovich, I.; Zhu, T.; Niu, N.; Wang, D.; Oliver, R.; Hu, E.L. Distinctive signature of indium gallium nitride quantum dot lasing in microdisk cavities. *Proc. Natl. Acad. Sci. USA* **2014**, *111*, 14042–14046. [[CrossRef](#)] [[PubMed](#)]
32. Li, Y.; Hu, X.; Song, Y.; Su, Z.; Jia, H.; Wang, W.; Jiang, Y.; Chen, H. The influence of temperature of nitridation and AlN buffer layer on N-polar GaN. *Mater. Sci. Semicond. Process.* **2022**, *141*, 106423. [[CrossRef](#)]
33. Lee, Y.-J.; Chiu, C.-H.; Ke, C.C.; Lin, P.C.; Lu, T.-C.; Kuo, H.-C.; Wang, S.-C. Study of the Excitation Power Dependent Internal Quantum Efficiency in InGaN GaN LEDs Grown on Patterned Sapphire Substrate. *IEEE J. Sel. Top. Quantum Electron.* **2009**, *15*, 1137–1143. [[CrossRef](#)]
34. Wang, H.; Ji, Z.; Qu, S.; Wang, G.; Jiang, Y.; Liu, B.; Xu, X.; Mino, H. Influence of excitation power and temperature on photoluminescence in InGaN GaN multiple quantum wells. *Opt. Express* **2012**, *20*, 3932–3940. [[CrossRef](#)] [[PubMed](#)]